*Desalination and Water Treatment*
www.deswater.com

doi: 10.5004/dwt.2017.20553

75 (2017) 213–224
May

# Adsorption of a cationic dye from aqueous solution using low-cost Moroccan diatomite: adsorption equilibrium, kinetic and thermodynamic studies

Mohamed Hadri[a,b], Zineb Chaouki[a], Khalid Draoui[b], Mostafa Nawdali[c], Abdeslam Barhoun[b], Hector Valdés[d], Nadjib Drouiche[e], Hicham Zaitan[a,*]

[a]*Laboratory LCMC, Faculty of Science and Technology, Sidi Mohamed Ben Abdellah University, B.P. 2202, Fez, Morocco, emails: hicham.zaitan@usmba.ac.ma (H. Zaitan), hadri.med.ch@gmail.com (M. Hadri), chaoukizineb90@gmail.com (Z. Chaouki)*
[b]*Laboratory MSI, Faculty of Sciences, Abdel Malek Essaadi University, B.P. 2121, M'hannech II, 93002, Tetouan, Morocco, emails: khdraoui@gmail.com (K. Draoui), a_barhoun@yahoo.fr (A. Barhoun)*
[c]*Laboratory LCMC, Polydisciplinary Faculty, Sidi Mohamed Ben Abdellah University, B.P 1223, Taza, Morocco, email: mostafa.nawdali@usmba.ac.ma*
[d]*Laboratorio de Tecnologías Limpias (F. Ingeniería), Universidad Católica de la Santísima Concepción, Alonso de Ribera 2850, Concepción, Chile, email: hvaldes@ucsc.cl*
[e]*Division CCSM, No. 2, Bd Dr. Frantz FANON- P.O. Box 140, Sept Merveilles, Algiers 16038, Algeria, email: drouichenadjib@crtse.dz*

Received 26 October 2016; Accepted 30 January 2017

**ABSTRACT**

This article presents the adsorption of Methylene Blue (MB) onto diatomite, in order to develop a low-cost treatment technology as a process alternative for dye removal. Diatomite used in this work was taken from the Nador area in the northeast of Morocco. Diatomite is characterised by different physical–chemical methods (X-ray diffraction, nitrogen adsorption-desorption isotherm, scanning electron microscopy and Fourier transform infrared). Results showed that the adsorption of MB onto diatomite mineral is affected by various operating parameters like contact time, initial dye concentration, adsorbent dosage, pH and temperature. Adsorption equilibrium is reached after 1.5 h of contact time. Maximum MB removal is obtained at pH = 12. MB removal rate decreases as pH decreases. Adsorption equilibrium data are fitted to Langmuir, Freundlich, Redlich–Peterson and Toth models. Adsorption data are well described by Langmuir isotherm model indicating that a homogeneous adsorption occurs. A maximum adsorption capacity (or monolayer coverage) of 11 mg $g^{-1}$ is obtained at 45°C. A value of the enthalpy of adsorption of 12.78 kJ $mol^{-1}$ is found confirming the endothermic nature of adsorption process, while a Gibb's free energy change ($\Delta G°$) falling in the range −30.8 to −35.34 kJ $mol^{-1}$ confirms the spontaneity of the process. Adsorption kinetics are fitted to a pseudo-second-order kinetic model. Experimental results indicate that the Moroccan diatomite could be used as a potential adsorbent for the removal of cationic dye molecules, at lower cost.

*Keywords:* Adsorption; Diatomite; Dye; Methylene Blue; Thermodynamic exploration

## 1. Introduction

Nowadays, a great variety of dyes are used in paper-making, textile, plastic, printing, food and pharmaceutical industries [1–3]. Coloured effluents from the textile and the dyestuff industries pose a serious environmental and health problem, because most of them are toxic, mutagenic and carcinogenic [4]. Therefore, the removal of dyes from wastewater streams to acceptable levels is a great challenge for the global chemical industry [5,6].

* Corresponding author.

Many techniques for wastewater treatment, including chemical precipitation, membrane separation, adsorption, photodegradation, bioremediation and electrochemical technologies, have been continuously developed to pursue efficient dye removal from wastewater [7–15]. Among all of them, adsorption process has been found to be superior in water reuse due to its low cost, design and operational simplicity [16,17].

A substantial number of adsorbents have been studied for the elimination of dye molecules from wastewater. Activated carbons have been a common choice as adsorbents in many industrial processes and have been found to exhibit great affinity for organic compounds [18–24]. However, the use of activated carbons as adsorbents is restricted due to its high operating costs and safety issues. Therefore, the development of effective and low-cost alternative adsorbents for the removal of dyes is attracting more and more attention from worldwide researchers [25].

In this context, natural minerals appear as interest adsorbents to clean polluted water, since their application could result in a cost-effective process for dye removal. Among natural minerals, diatomite is found as a quite abundant mineral in Morocco with low acquisition cost. Hence, diatomite is likely to become a strong candidate as adsorbent in the removal of dyes from aqueous solutions. However, there is a lack of information regarding the use of Moroccan diatomite as natural adsorbent in wastewater treatment. In this regard, the present study focuses on the feasibility to use Moroccan mineral as an adsorptive material in the removal of dyes from contaminated waters.

Methylene Blue (MB) is used here as a target organic pollutant, representatives of environmental relevance cationic dyes. The effects of operating parameters such as contact time, initial dye concentration, pH and temperature on the removal efficiency are evaluated. Different adsorption isotherms and kinetic models are employed to assess the adsorption process and to provide better understanding of adsorption characteristics and removal efficiencies.

## 2. Materials and methods

### 2.1. Materials

Diatomite was obtained from deposits located in the vicinity of Nador city, Morocco (denoted here as DT) and was used without any previous activation. Diatomite samples were dried at 110°C for 24 h and stored in a dessicator until further use. MB was supplied by HiMedia (HiMedia Laboratories, Mumbai, India). All chemicals used for analyses were of reagent grade obtained from Sigma-Aldrich (Sigma-Aldrich Chimie S.a.r.l., Lyon, France) and were used without further purification.

### 2.2. Characterisation of natural mineral

Specific surface area and pore volume were obtained from $N_2$ adsorption isotherms at –196°C, using a Micromeritics Asap 2010 sorptometer (Micromeritics Corporate Headquarters, USA). Mineralogical composition of diatomite was determined by X-ray diffraction analysis using X'Pert PRO Philips diffractometer (Philips Japan, Ltd., Japan), equipped with Cu K$\alpha$ radiation (l = 1.5406 Å). Bulk chemical composition was determined using an X-ray fluorescence (XRF) in a Bruker S4 Pioneer spectrometer (Bruker AXS GmbH Karlsruhe, Germany). Surface groups were identified using Fourier transform infrared (FTIR) spectroscopy in a VERTEX70 spectrophotometer (Bruker Optics S.a.r.l., France). FTIR spectra were recorded in the range of 4,000–400 $cm^{-1}$ with a 4 $cm^{-1}$ resolution. Surface morphology was registered by scanning electron microscopy (SEM; FEI-Philips XL30 ESEM, Corporate Headquarters, USA).

Basic and acid surface sites were determined by using the titration method [26]. A mass of 1 g DT sample was placed in 40 mL of the following solutions: NaOH (0.1 mol $L^{-1}$), $NaHCO_3$ (0.1 mol $L^{-1}$), HCl (0.1 mol $L^{-1}$) and $Na_2CO_3$ (0.05 mol $L^{-1}$). After that, vials were sealed and agitated for 24 h and then filtered. A volume of 10 mL of each filtrate were analysed by back titration using HCl or NaOH (0.1 mol $L^{-1}$). The total concentration of acidic sites were determined under the assumption that NaOH neutralises acidic sites of different strength (strong, mild and weak); $Na_2CO_3$ neutralises strong and mild acidic sites; and $NaHCO_3$ neutralises only strong acidic sites. The concentration of basic sites was calculated from the amount of hydrochloric acid consumed by the DT.

The pH value required to give net surface charge, designated as the pH of the point of zero charge ($pH_{pzc}$), was determined using the solid-adding method [27]. A volume of 20 mL of NaCl solution (0.1 mol $L^{-1}$) was transferred in series of flasks. Initial pH values were adjusted in the range of 2–12 by adding HCl or NaOH solutions. Then, 0.1 g of sample were weighed and placed into each bottle and stirred for 72 h at 20°C. The equilibrium pH was measured in each flask and plotted vs. the initial pH. The $pH_{pzc}$ was reported as the value at which the initial pH equals the equilibrium pH.

### 2.3. Batch adsorption experiments

MB adsorption experiments were carried out using the batch method. A mass of 20 mg of adsorbent was dispersed in 20 mL solution with an initial MB concentrations ranging from 0 to 1,000 mg $L^{-1}$ at pH = 6.6. The mixture was shaken (~200 rpm) until the equilibrium was reached using a water shaker bath. After that, the solid phase was separated from the liquid phase by centrifugation (5,000 rpm for 10 min). Finally, the residual concentration of MB was determined using a UV–visible spectrophotometer (UV2300II) by measuring the absorbance at $\lambda_{max}$ = 664 nm (Fig. 1).

Each experiment was conducted in triplicate to verify the reproducibility of the experience.

The total amount of adsorbed MB per gram of DT ($q$, mg $g^{-1}$) was determined from a mass balance as follows:

$$q = \frac{(C_0 - C)V}{m} \quad (1)$$

where $C_0$ (mg $L^{-1}$) and $C$ (mg $L^{-1}$) are MB concentrations at the beginning and at equilibrium or specific time, respectively. $m$ is the mass of adsorbent (g), and $V$ is the total volume of liquid (L).

The influence of operating conditions such as pH, contact time, dosage of adsorbent, initial concentration and

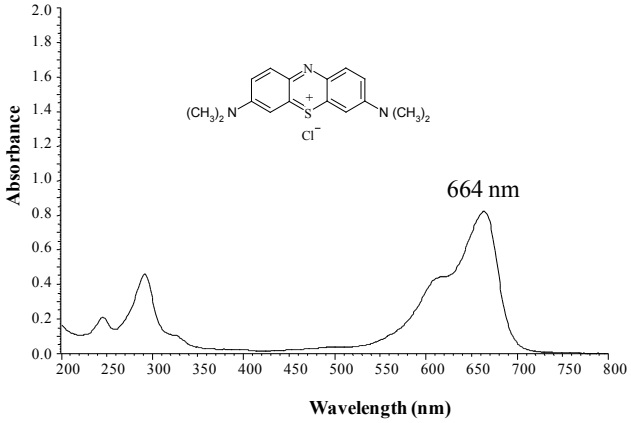


Fig. 1. UV–Vis spectrum of MB (MB concentration = 4.6 mg $L^{-1}$).

temperature on the adsorption of MB onto DT was studied in a batch system.

The effect of pH conditions on MB adsorption was conducted by varying the pH of the MB solution (30 mg $L^{-1}$) from 2.0 to 10 at 25°C. The initial pH was adjusted by adding HCl (0.1 mol $L^{-1}$) or NaOH (0.1 mol $L^{-1}$). The effect of the adsorbent mass on the adsorption of MB was performed by mixing different mass of DT with a fixed concentration of MB solution (100 mg $L^{-1}$). For examining the effect of initial MB concentration, 0.1 g of the DT was mixed with 50 mL of MB solutions with concentrations varying in the range of 0–40 mg $L^{-1}$ at 25°C, without pH adjusting. The effect of temperature on MB adsorption was investigated at four different temperatures (15°C, 25°C, 35°C and 45°C).

## 3. Results and discussion

### 3.1. Characterisation of diatomite mineral

Figs. 2(a) and (b) and Table 1 summarise the textural properties of DT mineral obtained from $N_2$ adsorption–desorption isotherms at –196°C. Nitrogen adsorption onto DT follows a type IV isotherm according to the IUPAC classification. The initial part of the type IV isotherm ($P/P_0 < 0.4$) corresponds to the monolayer region, and it is scarcely visible, which could be ascribed to physical adsorption at the surface of the adsorbent. In the high relative pressure range, a hysteresis loop is observed and could be associated to capillary condensation of the adsorbate in the mesopores structures, formed between the elementary mineral particles named tactoids [28]. A hysteresis between the adsorption and desorption curves is also registered. As shown in Table 1, BET surface area of the DT mineral is 17.36 $m^2$ $g^{-1}$. Pore size distribution indicates that DT material has a fraction of micropores with an average size of 1.94 nm.

XRD results shown in Fig. 3 indicate that the DT mineral is poorly crystallised and mainly composed by silica ($SiO_2$) with some $Al_2O_3$, $Fe_2O_3$ and CaO. The amorphous band may be attributed to the glass formation of $SiO_2$. Peaks at 21°, 26° and 39° are characteristic of diatomite mineral [29].

XRF results (Table 2) reveal that DT mineral is mainly composed of $SiO_2$, $Al_2O_3$ and CaO and trace amount of other oxides such as MgO, $K_2O$, $Na_2O$, $TiO_2$ and $Fe_2O_3$.

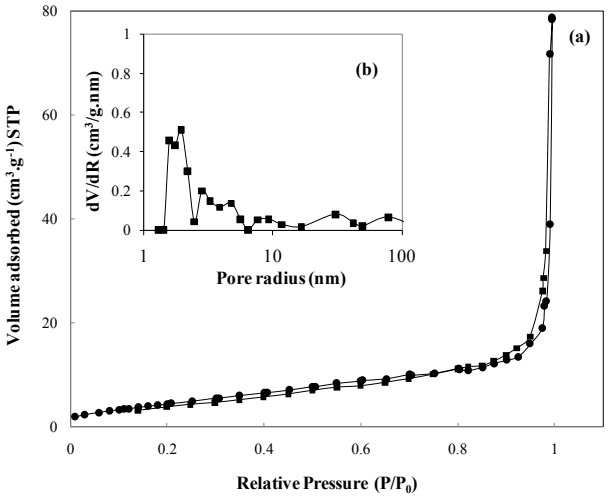


Fig. 2. (a) $N_2$ adsorption–desorption isotherm of DT mineral at 77 K and (b) BJH pore size distribution.

Table 1
Physical characterisation of DT mineral

| Parameter | Value |
|---|---|
| $S_{BET}$ ($m^2$ $g^{-1}$) | 17.36 |
| $V_t$[a] ($cm^3$ $g^{-1}$) | 0.06 |
| $V_{meso}$[b] ($cm^3$ $g^{-1}$) | 0.04 |
| $S_{ext}$[c] ($m^2$ $g^{-1}$) | 12.92 |
| $S_{micro}$[d] ($m^2$ $g^{-1}$) | 4.44 |
| $V_{micro}$[e] ($cm^3$ $g^{-1}$) | 0.02 |
| $D_p$[f] (nm) | 1.94 |

[a]Total pore volume.
[b]Mesoporous volume.
[c]External specific surface.
[d]Specific micropore surface area.
[e]Microporous volume.
[f]Pore diameter.

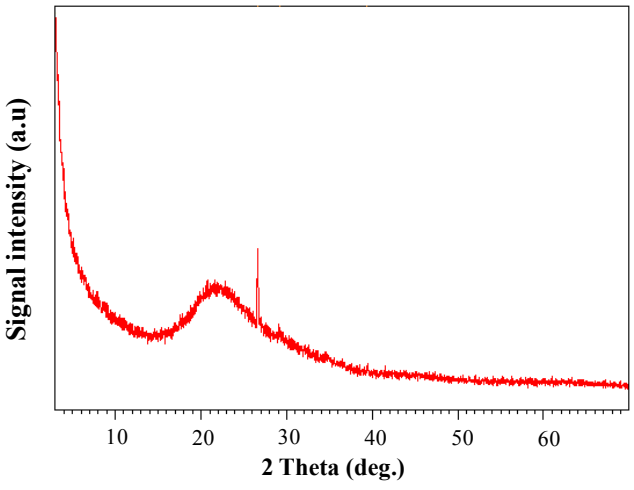


Fig. 3. XRD of DT mineral.

FTIR results depicted in Fig. 4 show IR vibrations at 3,425 and 1,631 $cm^{-1}$, corresponding to O–H stretching vibrations and adsorbed water, respectively. The IR bands registered at 467 and 1,050 $cm^{-1}$ may be attributed to asymmetric stretching modes of Si–O–Si bonds [30]. The band at 796 $cm^{-1}$ could correspond to the Si–O–Al stretching vibration [31].

These results are in agreement with those obtained by XRF analysis. Silanol groups (Si–OH) are spread over the diatomite surface. This is a very active surface group, which could interact with polar organic compounds as MB during the adsorption process.

Table 2
Chemical composition of DT mineral obtained by XRF analysis (wt%)

| Component | Composition (%w) |
|---|---|
| $SiO_2$ | 72.8 |
| $Al_2O_3$ | 5.22 |
| $Fe_2O_3$ | 1.94 |
| MgO | 1.13 |
| $K_2O$ | 0.901 |
| CaO | 5.86 |
| $Na_2O$ | 0.83 |
| $TiO_2$ | 0.27 |

Fig. 5 displays textural characteristics of DT mineral obtained by SEM analysis. SEM images show that diatom frustules are well preserved, having disk and cylindrical shapes with diameter less than 20 μm. Frustules occur as hosted assemblages in a clayey ground mass. It is also noticed that the surface of the raw diatomite is irregular and contains pores of different sizes and shapes, which could provide a surface area for the adsorption of pollutants.

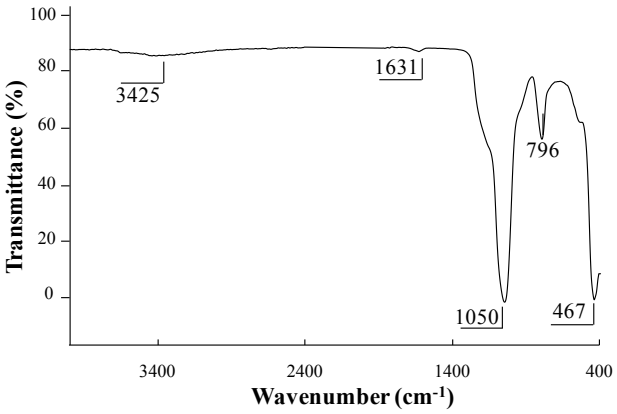


Fig. 4. FTIR spectrum of DT mineral.

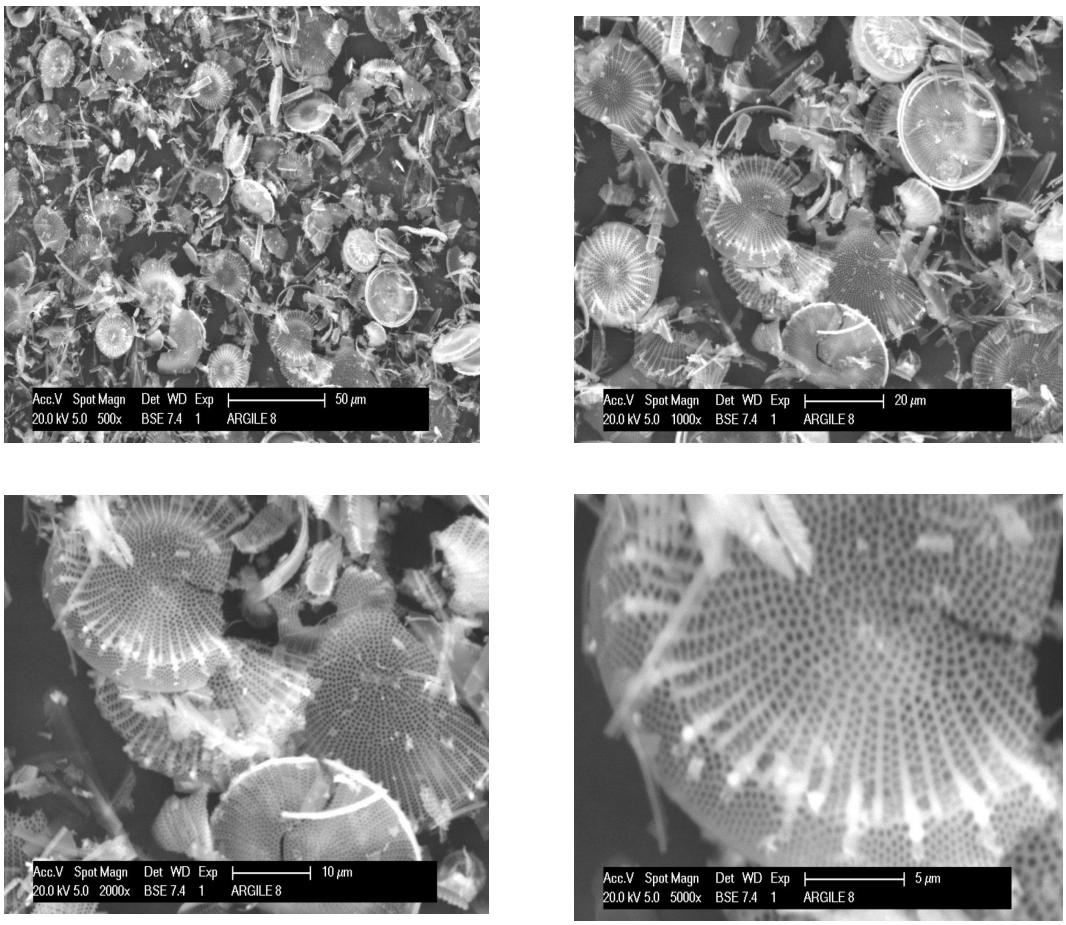


Fig. 5. SEM images of the DT mineral.

Acid and basic properties of DT mineral are listed in Table 3. It can be observed that the amount of acidic groups is significantly higher than the amount of basic groups. These results suggest that diatomite mineral has an acidic character. These results are in agreement with $pH_{pzc}$ value previously measured ($pH_{pzc}$ = 6.5).

### 3.2. Effect of contact time and adsorption kinetics

Adsorption kinetics must be investigated in order to determine the time necessary for reaching equilibrium and to elucidate the mechanism of the adsorption process. The rate of MB adsorption on the DT sample was studied by measuring the adsorption amount as a function of time, keeping constant the volume ($V$ = 200 mL), the initial concentration ($C_0$ = 25 mg $L^{-1}$) and the mass of adsorbent per liter of aqueous solution ($R$ = 2 g $L^{-1}$). Fig. 6 illustrates the adsorbed amount of MB as a function of the contact time. Non-linear fit of pseudo-first-order, pseudo-second-order and Elovich models to kinetic data is also shown in Fig. 6, whereas the coefficient of determination ($R^2$) and kinetic parameters are listed in Table 4.

Results indicate that a fast initial adsorption occurs in the first minutes (0–90 min), where 85% MB removal takes place, which may be due to electrostatic (columbic) attractions between the negatively charge surface of DT (hydroxyl groups) and the cationic charge of MB molecule. After that, the adsorption increases slowly with the time, until equilibrium is reached after 90 min. After 3 h of contact time, almost all of the available active sites on the diatomite surface are saturated, and the adsorption capacity does not change anymore with time. Therefore, 3 h is selected as the time needed to reach the MB adsorption equilibrium in further adsorption experiments. FTIR results discussed before showed that diatomite surface contains X–OH groups (Si–OH silanol and Al–OH aluminol groups), which could act as active centres in the adsorption of cationic basic dyes as MB molecule. Hence, the change in the rate of adsorption might be due to fact that initially all the active adsorption sites (Si–OH and Al–OH groups) are vacant, and there is a very high solute concentration gradient. Later, the lower adsorption rate is due to a decrease in the number of vacant adsorption sites and MB concentration. The decreased in the adsorption rate, particularly, at the end of experiments, indicates the possible monolayer formation of MB on the adsorbent surface [32]. This may be attributed to the lack of available active sites required for further uptake after the equilibrium is attained.

Modeling of the adsorption kinetics is useful in the prediction of the adsorption mechanism of pollutants onto solid surfaces. Adsorption kinetic models, namely

Table 3
Acidic and basic surface properties of DT mineral

| Site content (mmol $g^{-1}$) | Value |
|---|---|
| Strong acidic sites (mmol $g^{-1}$) | 0.0 |
| Mild acidic sites (mmol $g^{-1}$) | 2.10 |
| Weak acidic sites (mmol $g^{-1}$) | 0.55 |
| Total acidic sites (mmol $g^{-1}$) | 2.65 |
| Total basic sites (mmol $g^{-1}$) | 0.43 |
| Total sites (mmol $g^{-1}$) | 3.08 |

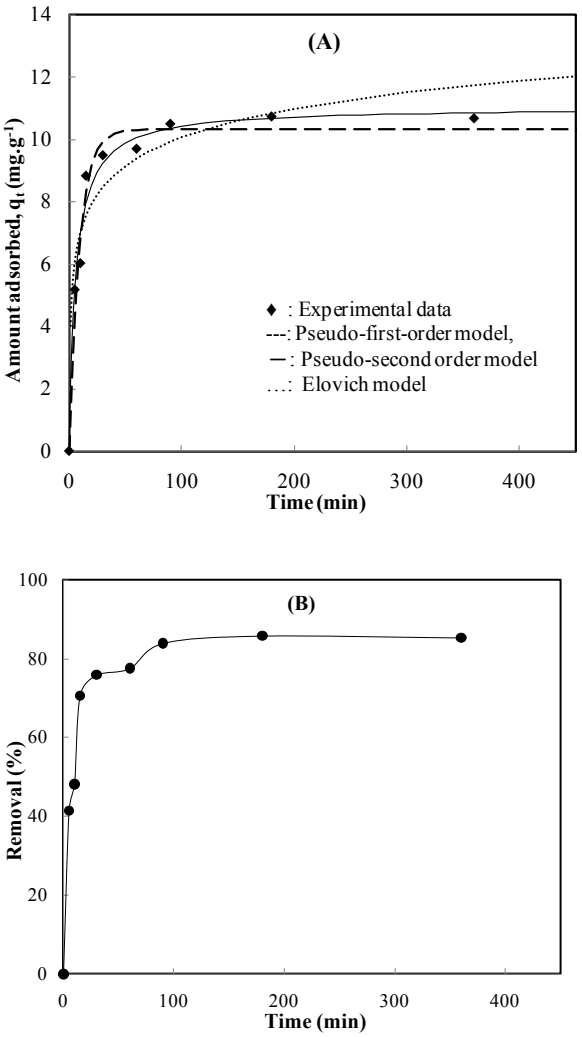


Fig. 6. Effect of contact time on the adsorption of MB: (A) adsorbed amount of MB per mass of diatomite mineral and (B) MB removal (experimental conditions: initial MB concentration: 25 mg $L^{-1}$, diatomite dose: 2 g $L^{-1}$, temperature: 25°C, agitation speed: 200 rpm).

Table 4
Kinetic parameters for the adsorption of MB onto DT mineral

| Kinetic model | Parameters | Values |
|---|---|---|
| Pseudo-first-order | $q_{exp}$ (mg $g^{-1}$) | 10.75 |
| | $q_e$ (mg $g^{-1}$) | 10.320 |
| | $k_1$ ($min^{-1}$) | 0.111 |
| | $R^2$ | 0.970 |
| Pseudo-second-order | $q_e$ (mg $g^{-1}$) | 11.034 |
| | $k_2$ (g $mg^{-1}$ $min^{-1}$) | 0.015 |
| | $R^2$ | 0.99 |
| Elovich | $\alpha$ (mg $g^{-1}$ $min^{-1}$) | 0.763 |
| | $\beta$ (g $mg^{-1}$) | 28.370 |
| | $R^2$ | 0.93 |

pseudo-first-order, pseudo-second-order, Elovich and intraparticle diffusion models, are used in this work to describe the adsorption kinetics of MB onto the DT adsorbent.

The pseudo-first-order kinetic model [33] is given as:

$$q_t = q_e(1-\exp(-k_1 t)) \quad (2)$$

where $q_t$ and $q_e$ (mg g$^{-1}$) are the adsorption capacity at time $t$ and equilibrium time, respectively, and $k_1$ (min$^{-1}$) is the pseudo-first-order model rate constant. Pseudo-first-order constants of the kinetic model are obtained by plotting $q_t$ vs. $t$. Results are presented in Table 4.

The pseudo-second-order kinetic model by Ho et al. [34] is given as:

$$q_t = \frac{k_2 q_e^2 t}{1+k_2 q_e t} \quad (3)$$

where $k_2$ (g mg$^{-1}$ min$^{-1}$) is the adsorption rate constant.

Elovich kinetic model is given as:

$$q_t = \frac{1}{\beta}\ln\alpha\beta + \frac{1}{\beta} lnt \quad (4)$$

where $\alpha$ is initial adsorption rate constant, and $\beta$ is desorption rate constant. The fitting of the models is evaluated using the coefficient of determination ($R^2$).

According to Table 4, the adsorption process can be described by the pseudo-second-order kinetic model. In fact this model shows a coefficient of determination ($R^2$ ~ 0.99) higher than that the pseudo-first-order and the Elovich model and closeness of $q_{exp}$, experimental to $q_e$, theoretical value.

The applicability of the pseudo-second-order model suggests that chemical interactions are responsible for the adsorption of MB on DT [35].

Additionally analysis of the adsorption kinetics data allows to determine whether intraparticle diffusion could be the rate-limiting step in the adsorption mechanism and to calculate the corresponding rate constant ($k_{pi}$). The adsorption mechanism of MB onto DT could be described by a sequence of: (1) external diffusion of the adsorbate through the boundary layer that surrounds the adsorbent external surface, (2) pore or intraparticle diffusion and (3) the adsorption of the adsorbate onto active sites present on the solid surface [36,37]. Hence, the investigation of the importance of these steps in the adsorption process is evaluated by using the intraparticle diffusion model [38]:

$$q_t = k_{pi} t^{1/2} + C_i \quad (5)$$

where $k_{pi}$ and $C_i$ are intraparticle diffusion rate constant (mg g$^{-1}$ min$^{-1/2}$) and a constant (mg g$^{-1}$), respectively. When the plot of amount of MB adsorbed ($q_t$) vs. $t^{1/2}$ is linear and passes through the origin, the adsorption process follows the intraparticle diffusion mechanism, which is controlled by only internal diffusion [39]. However, if the data exhibit multi-linear plots, then two or more steps influence the adsorption process.

Fig. 7 shows that MB adsorption onto DT mineral exhibits three different stages. The first stage with a higher slope ($k_{p1}$ = 2.17 mg g$^{-1}$ min$^{-1/2}$, see Table 5) starts from the origin and represents the external diffusion, which is related to the MB transfer through the external surface of DT. This step is achieved in <15 min. The second stage is more gradual and can be attributed to intraparticle diffusion, showing a decrease in the slope ($k_{p2}$ = 0.268 mg g$^{-1}$ min$^{-1/2}$) due to the gradual increase in the adsorption rate. Finally, the third stage corresponds to the adsorption equilibrium, which is linear ($k_{p3}$ = 0.001 mg g$^{-1}$ min$^{-1/2}$). Here, the intraparticle diffusion is attenuated, and the equilibrium is achieved due to a decrease in the concentration of MB in the solution [39].

It can be inferred that the linearity of the intraparticle diffusion model does not completely obey due to the existence of more than one controlling stage in the whole process (Fig. 7). The lines corresponding to the second and third stages do not pass through the origin, indicating that intraparticle mass transfer resistance is not the only rate-limiting step in the adsorption mechanism; thus, other factors may influence the adsorption kinetics [37].

### 3.3. Effect of the adsorbent dose and the initial concentration of MB

Fig. 8 shows the effect of the adsorbent dosages on the adsorption capacity of DT and removal efficiency towards MB. Experiments were carried out in the range 0.2–1.2 g of DT, using an MB solution with an initial concentration of 100 mg L$^{-1}$ at pH = 6 and 25°C, during 3 h of contact time.

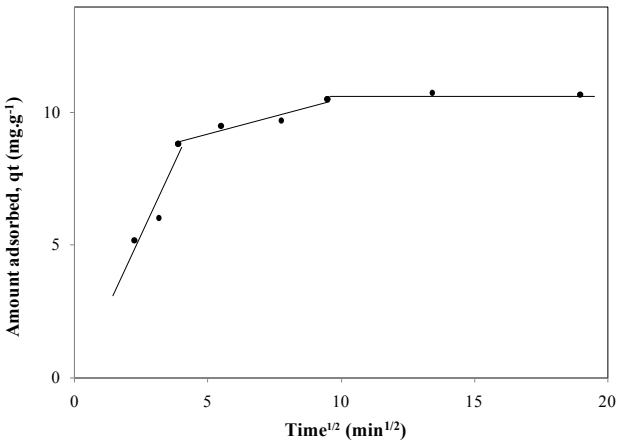


Fig. 7. Application of the intraparticle diffusion model to the adsorption of MB onto DT mineral (experimental conditions: initial MB concentration: 25 mg L$^{-1}$, diatomite dose: 2 g L$^{-1}$, agitation speed: 200 rpm, temperature: 25°C).

Table 5
Parameters and coefficient determinations of the intraparticle diffusion model for the adsorption of MB onto DT

| 1st stage | | | 2nd stage | | | 3rd stage | | |
|---|---|---|---|---|---|---|---|---|
| $K_{p1}$ | $C_1$ | $R^2$ | $K_{p2}$ | $C_2$ | $R^2$ | $K_{p3}$ | $C_3$ | $R^2$ |
| 2.17 | 0.02 | 0.87 | 0.268 | 7.85 | 0.99 | 0.001 | 10.6 | 0.42 |

As it can be seen in Fig. 8, the removal efficiency rises from 31% to 99% with the increase on the adsorbent mass. This can be attributed not only to an increase on the adsorbent surface area but also to higher availability of adsorption actives sites. However, with a further mass increase, the removal efficiency does not change due that all MB molecules have already been removed from the solution [40]. It can also be observed that the adsorption capacity of DT towards MB in the range between 0.6 and 0.2 g reaches a maximum adsorption capacity. At a lower mass content, DT adsorption sites are completely covered, reaching the saturation and limiting a further MB adsorption. A different effect is observed at higher adsorbent dose. Under such conditions, there are adsorption sites still available for MB adsorption to take place.

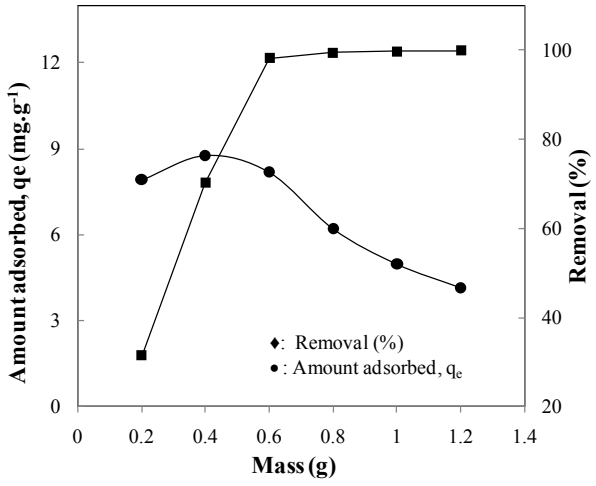


Fig. 8. Effect of adsorbent dose on MB removal (experimental conditions: pH: 6, initial MB concentration: 100 mg $L^{-1}$, diatomite amount: 0.2–1.2 g, contact time: 3 h, agitation speed: 200 rpm, temperature: 25°C).

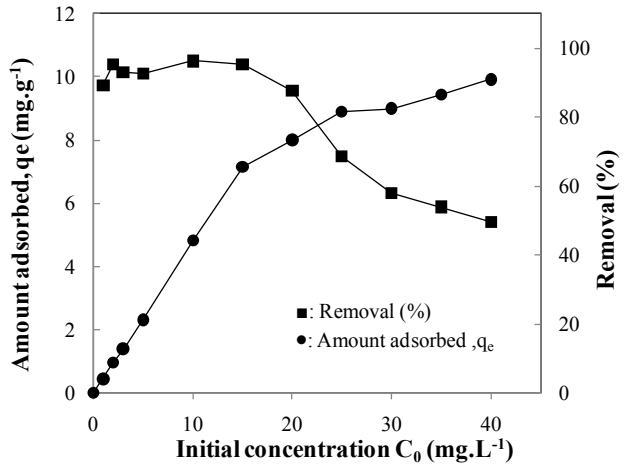


Fig. 9. Effect of the initial concentration of MB on the adsorption removal (experimental conditions: pH: 6, initial MB concentration: 0–40 mg $L^{-1}$, diatomite dose: 2 g $L^{-1}$, contact time: 3 h, agitation speed: 200 rpm, temperature: 25°C).

Fig. 9 depicts the effect of the initial concentration of MB on MB removal onto DT mineral. Experiments were carried out using an initial concentration of MB in the range between 0 and 40 mg $L^{-1}$ at pH = 6 and 25°C. It has to be noticed that in this case the concentration of DT is kept the same value (2 g $L^{-1}$) in all experiments. It can be seen that the adsorption amount (mg $g^{-1}$) increases and the adsorption percentage decreases as increasing initial adsorbate concentration. The higher initial adsorbate concentration provides a significant driving force to overcome mass transfer resistance for adsorbate transportation between the solution and the surface of adsorbent, which increased the adsorption amount. On the other hand, the higher adsorbate concentrations induced a saturation of the active adsorption sites on adsorbent surface. In other words, active adsorption sites are less available for adsorbate binding at higher concentrations, which decreased the adsorption percentage [41].

### 3.4. Effect of pH

The pH of the solution is normally considered as a major controlling factor in adsorbate–adsorbent interaction. Experiments were carried out using an initial concentration of MB of 30 mg $L^{-1}$, 2 g $L^{-1}$ of diatomite suspension at 25°C and in a pH range of 2.0–12.0 as it displayed in Fig. 10.

Experimental results indicate that pH considerably influences MB adsorption efficiency, particularly at pH values higher than $pH_{pzc}$. Adsorption interactions among active surface sites and MB molecules change along with pH. Maximum MB removal takes place at basic pH (pH = 8–12), and decreases as the pH decrease. At pH < $pH_{pzc}$, surface hydroxyl groups will be in their protonated form (X–OH + $H^+ \rightarrow X–OH_2^+$) with (X = Si or Al) [42], which results in a low adsorption efficiency due to possible electrostatic repulsion between the positively charged of DT surface (excess hydrogen ions ($H^+$)) and basic MB [43]. On the other hand, at pH > $pH_{pzc}$, surface hydroxyl groups on the DT will be in their deprotonated form (X–OH + $OH^- \rightarrow X–O^- + H_2O$) [30,44], increasing electrostatic interactions between $MB^+$ and

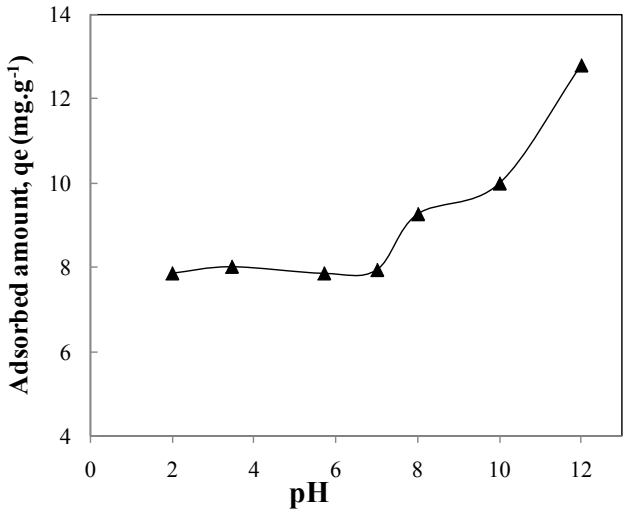


Fig. 10. Effect of pH on the adsorption of MB onto DT (experimental conditions: initial MB concentration: 30 mg $L^{-1}$, diatomite dose: 2 g $L^{-1}$, contact time: 3 h, agitation speed: 200 rpm, temperature: 25°C).

the negative charge of diatomite surface (X–O⁻), leading to higher removal of MB.

### 3.5. Adsorption isotherms

Adsorption isotherms are usually carried out to get necessary information for optimisation, scale up and final design of the adsorption systems [45]. Adsorption isotherms represent the relationship between the amount adsorbed per unit mass of adsorbent and the amount of adsorbate that remains in the solution when the equilibrium is reached [46].

In this work, experimental data of the adsorption of MB onto DT are fitted to several adsorption isotherm models (Fig. 11(a)) as Langmuir [47], Freundlich [48], Redlich–Peterson and Toth [49,50], which have been intensively used to describe the adsorption equilibrium of organic pollutants onto several kinds of adsorbents [46,48–50]. Table 6 lists the calculated parameters and coefficient of determinations of each model using a non-linear regressive method. Adsorption isotherm models express the adsorbed quantity of MB per mass of DT, $q_e$ (mg g$^{-1}$), as a function of MB concentration at the equilibrium, $C_e$ (mg L$^{-1}$), as follows:

Langmuir equation:

$$q_e = \frac{K_L C_e q_m}{1 + K_L C_e} \tag{6}$$

where $q_m$ (mg g$^{-1}$) is the maximum adsorption capacity of adsorbent that is related to the monolayer adsorption capacity, and $K_L$ (L mg$^{-1}$) is the Langmuir adsorption equilibrium constant related to the affinity of the binding sites (L mg$^{-1}$).

The affinity between DT and MB is evaluated based on the separation factor, $R_L$, determined from the Langmuir adsorption isotherm model [51,52]. The value of $R_L$ is calculated using Eq. (7):

$$R_L = \frac{1}{1 + K_L C_0} \tag{7}$$

where $C_0$ (mg L$^{-1}$) is the initial concentration of MB, and $K_L$ (L mg$^{-1}$) is the Langmuir constant related to the energy of adsorption. If the $R_L$ value is >1, the adsorption process is unfavourable. Whether the $R_L$ value is equal to 1 or the value

Table 6
Langmuir, Freundlich, Toth and Redlich–Peterson parameters for MB adsorption onto DT mineral

| Models | Isotherms parameters | Values |
|---|---|---|
| Langmuir | $q_m$ (mg g$^{-1}$) | 9.15 |
| | $K_L$ (L mg$^{-1}$) | 1.3 |
| | $R^2$ | 0.96 |
| Freundlich | $K_F$ ((mg g$^{-1}$) (L mg$^{-1}$)$^{1/n}$) | 3.81 |
| | $N$ | 3.18 |
| | $R^2$ | 0.83 |
| Toth | $q_m'$ (mg g$^{-1}$) | 8.5 |
| | $K_T$ ((mg L$^{-1}$)$^{t'}$) | 0.76 |
| | $T$ | 3 |
| | $R^2$ | 0.93 |
| Redlich–Peterson | $K_{RP}$ (L mg$^{-1}$)$^{-g}$ | 7.004 |
| | $a_{RP}$ (L g$^{-1}$) | 0.454 |
| | $G$ | 1.19 |
| | $R^2$ | 0.85 |

Note: $q_m$: maximum adsorption capacity; $K_L$: adsorption equilibrium constant or Langmuir coefficient; $q_m'$: maximum monolayer adsorption capacity parameter, $b'$: Toth isotherm constant, $t$: a dimensionless constant; $k$: adsorption equilibrium constant; and $n$: empirical constant of the Freundlich model. $K_{RP}$, $a_{RP}$, and $g$ are Redlich–Peterson constants.

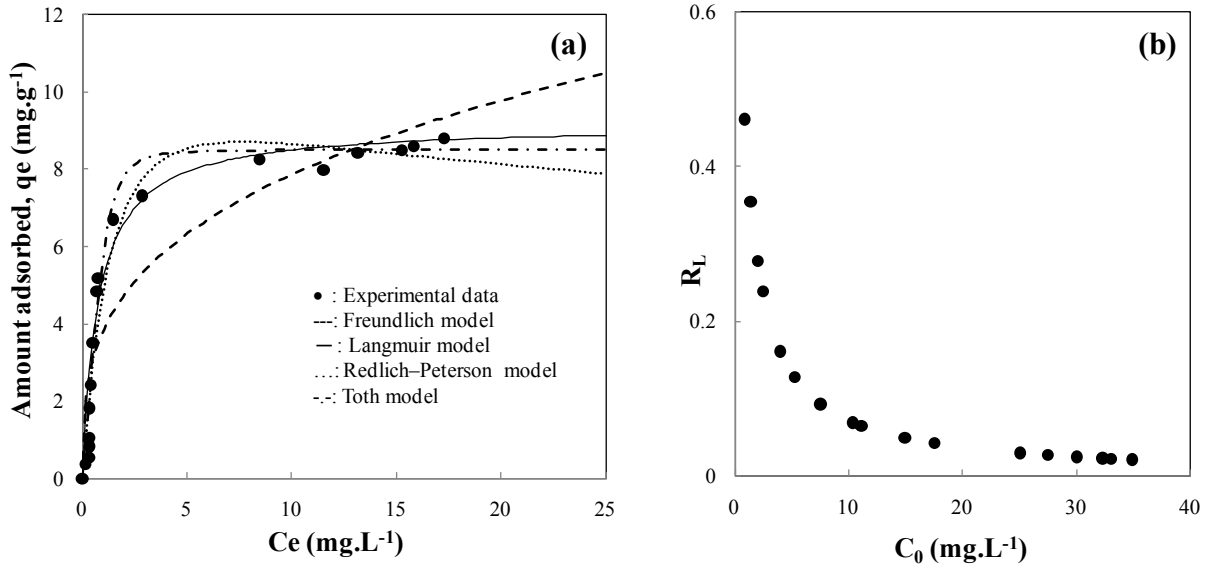


Fig. 11. Equilibrium data of MB adsorption onto DT mineral: (a) model fitting to different adsorption models and (b) separation factor ($R_L$) (experimental conditions: diatomite amount: 0.1 g, contact time: 3 h, agitation speed: 200 rpm, temperature: 25°C).

lies in between 0 and 1 indicates that the adsorption is linear and favourable. $R_L$ = 0 indicates irreversible adsorption process [53]. The dependence of $R_L$ on the investigated concentrations (1–35 mg $L^{-1}$) is shown in Fig. 11(b). As it can be seen, the $R_L$ values ranged from 0.015 to 0.38, indicating that the adsorption process of MB onto DT occurs favourably in this concentration range.

Freundlich equation:

$$q_e = K_F C_e^{1/n} \tag{8}$$

where $K_F$ ((mg $g^{-1}$) (L $mg^{-1})^{1/n}$) stands for the adsorption equilibrium constant, and $n$ is the empirical constant of the Freundlich model.

Toth equation:

Toth isotherm is a semi-empirical expression, normally used to describe a monolayer adsorption. Parameters given in this equation are used to characterise surface heterogeneity and interactions of adsorbed molecules. It is a three-parameter model usually written as follows:

$$q_e = \frac{q_m' K_T C_e}{\left[K_T + C_e^t\right]^{1/t}} \tag{9}$$

where $q_m'$ (mol $kg^{-1}$) is the maximum monolayer adsorption capacity parameter; $K_T$ ((mg $L^{-1})^t$) is the Toth isotherm constant, and $t$ is a dimensionless constant, usually less than unity. Parameters $K_T$ and $t$ are specifics for the adsorbate–adsorbent systems. The more parameter $t$ is away from unity, the more heterogeneous is the system. Parameters $q_e$, $K_T$, and $t$ in Eq. (9) were determined numerically.

Redlich–Peterson equation:

The Redlich–Peterson isotherm model is a three-parameter empirical model, which consists of both Langmuir and Freundlich isotherm models. Due to the versatility of this isotherm model, it can be used for either homogeneous or heterogeneous systems. It can be represented by Eq. (10):

$$q_e = \frac{K_{RP} C_e}{1 + a_{RP} C_e^g} \tag{10}$$

where $K_{RP}$, $a_{RP}$ and $g$ are Redlich–Peterson constants.

As it can be observed in Fig. 11(a), a solid line shows that experimental data fit very well the Langmuir adsorption model. Additionally, experimental data are also fitted to other common isotherm models, such as: Freundlich, Redlich–Peterson and Toth equations. The Langmuir model give the best fit as it is indicated by the relative high value of $R^2$ ($R^2$ ~ 0.96; see Table 6 and Fig. 11(a)).

As it can be seen in Fig. 11, the amount of adsorbed MB on DT at 15°C reaches a plateau at 9.15 mg $g^{-1}$. This result is in excellent agreement with the observed values using other porous adsorbents such as fly ash (9.81 mg $g^{-1}$) [54], activated carbon made from rice husk (9.73 mg $g^{-1}$) [55], clay (6.3 mg $g^{-1}$) [56], raw and calcined kaolinite (8.88 and 7.59 mg $g^{-1}$) [57], zeolite (10.82 mg $g^{-1}$) [58], amorphous silica (22.66 mg $g^{-1}$) [58], natural ilittic clay mineral (24.87 mg $g^{-1}$) [59], residue biochar (16.75 mg $g^{-1}$) [60], activated saw dust (4.58 mg $g^{-1}$) [61], wheat shells (16.56 mg $g^{-1}$) [62], *Posidonia oceanica* (L.) fibres (5.56 mg $g^{-1}$) [63] and parthenium (SWC) natural tripoli (16.62 mg $g^{-1}$) [64].

Moreover, considering that DT has an average price around 0.04–0.12·US$ $kg^{-1}$, the use of this material yields an additional advantage in terms of operating costs which is 500 times lower than of the activated carbon (20·US$ $kg^{-1}$) [28]. Thus, diatomite mineral is likely to become a strong adsorbent candidate for dyes removal, as an alternative adsorbent to activated carbons due to its easy availability, low cost and good adsorption properties.

The feasibility of using diatomaceous earth in the removal of problematic reactive dyes has been also investigated by Al-Ghouti et al. [65]. They showed that natural diatomite may be a promising adsorbent from environmental and purification point of views.

### 3.6. Effect of temperature

As a way of illustration, Fig. 12 shows the effect of temperature on the adsorption of MB onto DT material. As it can be seen, the adsorption capacity of DT natural mineral towards MB progressively increases when temperature raises from 15°C to 45°C.

MB adsorption is increased around an 18% with the increase on temperature suggesting that the adsorption of MB onto DT natural mineral is an endothermic process. This was attributed to the activation of the adsorbent surface and the increase of the intraparticle diffusion of MB as the temperature increased [58].

### 3.7. Adsorption thermodynamics

In order to evaluate the effect of temperature, the thermodynamic feasibility and the spontaneous nature of the adsorption process of the MB–DT adsorption, the experiments were performed with MB concentration of 0–30 mg $L^{-1}$ at 15°C, 25°C, 35°C and 45°C.

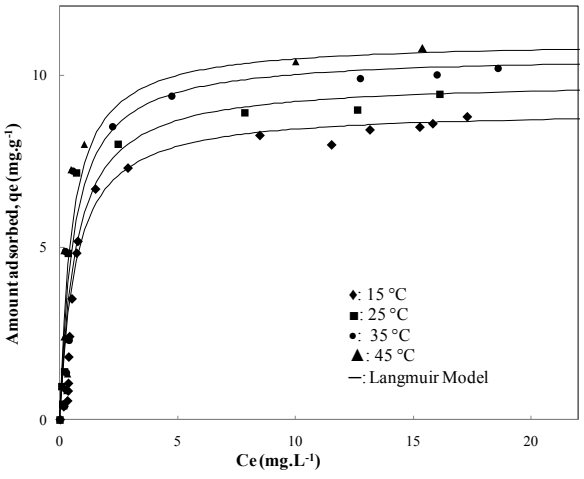


Fig. 12. MB adsorption isotherms of DT at different temperatures (experimental conditions: diatomite amount: 0.1 g, contact time: 3 h, agitation speed: 200 rpm, temperature: 15°C–45°C).

Table 7
Thermodynamic parameters for the MB adsorption on DT

| Temperature (°C) | Parameters | | |
|---|---|---|---|
| | $\Delta G°$ (kJ mol$^{-1}$) | $\Delta H°$ (kJ mol$^{-1}$) | $\Delta S°$ (kJ mol$^{-1}$ K$^{-1}$) |
| 15 | –30.80 | 12.78 | 0.15 |
| 25 | –32.31 | | |
| 35 | –33.82 | | |
| 45 | –35.34 | | |

The Gibb's free energy change ($\Delta G°$ (kJ mol$^{-1}$)), enthalpy change $\Delta H°$ (kJ mol$^{-1}$) and the entropy change $\Delta S°$ (kJ mol$^{-1}$ K$^{-1}$) of the MB adsorption were calculated using the following equations [66].

$$\Delta G^{\circ} = -RT\ln K = \Delta H^{\circ} - T\Delta S^{\circ} \quad (11)$$

$$\ln K = \Delta S°/R - \Delta H°/RT \quad (12)$$

where $K$ is the thermodynamic equilibrium constant; $R$ (8.314 J mol$^{-1}$ K$^{-1}$) is the universal gas constant; and $T$ (K) is the temperature.

Table 7 shows the calculated thermodynamic parameters for MB–DT adsorption. The negative values of ΔG° indicate that adsorption process is spontaneous and thermodynamically favourable [67,68].

Furthermore, $\Delta G°$ values are more negatives with increasing temperature, suggesting that adsorption is more favourable at higher temperature. The positive value of $\Delta H°$ (12.78 kJ mol$^{-1}$) indicated endothermic nature of the adsorption [69] and that the adsorption of MB onto DT is physical in nature [70].

## 4. Conclusions

DT could be effectively used as a low-cost natural mineral in the removal of cationic dyes from contaminated waters. Results show that the adsorption process takes place very rapidly in the first minutes. Then, it is followed by a slower rate that gradually approaches a plateau. Adsorption equilibrium is reached after 3 h of contact time. The kinetics of MB adsorption onto DT is well represented by a pseudo-second-order kinetic model. Experimental results indicate that adsorption interactions among active surface sites and MB molecules are pH dependences. At pH < $pH_{pzc}$, DT adsorption capacity towards MB is reduced. This could be related to electrostatic repulsion between the positively charged of DT surface and positive charge of MB molecule. At pH > $pH_{pzc}$, DT adsorption capacity towards MB is increased. Under this pH conditions, an increase in electrostatic interactions between positive charged MB molecules and deprotonated hydroxyl surface groups of diatomite leads to higher removal of MB. The optimum adsorption was obtained at basic (pH = 8–12). The adsorption yield increases with the increase of adsorbent dosage and the initial concentration. The adsorption isotherm showed that Langmuir model had a better fit to the experimental data, and the maximum adsorption capacity is found to be 11 mg g$^{-1}$ at 45°C.

The thermodynamic studies reveal that the adsorption of MB onto DT mineral is spontaneous and endothermic under examined conditions. Furthermore, based on all results, it can be also concluded that the natural mineral could be effectively applied as an alternative low-cost adsorbent to remove toxic organic pollutants from wastewaters.

## Symbols

| | | |
|---|---|---|
| $C_0$ | — | MB concentrations at the beginning |
| $C$ | — | MB concentrations at equilibrium or specific time |
| $m$ | — | Mass of adsorbent |
| $V$ | — | Total volume of liquid |
| $S_{BET}$ | — | Specific surface |
| $V_t$ | — | Total pore volume |
| $V_{meso}$ | — | Mesoporous volume |
| $S_{ext}$ | — | External specific surface |
| $S_{micro}$ | — | Specific micropore surface area |
| $V_{micro}$ | — | Microporous volume |
| $D_p$ | — | Pore diameter |
| $q_t$ | — | Adsorption capacity at time $t$ |
| $q_e$ | — | Adsorption capacity at equilibrium time |
| $k_1$ | — | Pseudo-first-order model rate constant |
| $\alpha$ | — | Initial adsorption rate constant |
| $\beta$ | — | Desorption rate constant |
| $q_m$ | — | Maximum adsorption capacity of adsorbent |
| $K_L$ | — | Langmuir model constant |
| $K_F$ | — | Adsorption equilibrium constant |
| $n$ | — | Empirical constant of the Freundlich model |
| $q_m'$ | — | Maximum monolayer adsorption capacity parameter |
| $K_T$ | — | Toth isotherm constant |
| $t$ | — | Dimensionless constant |
| $K_{RP}$ | — | Redlich–Peterson constant |
| $a_{RP}$ | — | Redlich–Peterson constant |
| $g$ | — | Redlich–Peterson constant |
| $\Delta G°$ | — | Gibb's free energy change |
| $\Delta H°$ | — | Enthalpy change |
| $\Delta S°$ | — | Entropy change |

## Acknowledgement

This work was supported by the Morocco Ministry of Environment of DE-LIX Project to whom the authors are grateful.

## References

[1] D. Pokhrel, T. Viraraghavan, Treatment of pulp and paper mill wastewater – a review, Sci. Total Environ., 333 (2004) 37–58.
[2] O. Tünay, I. Kabdasli, G. Eremektar, D. Orhon, Color removal from textile wastewaters, Water Sci. Technol., 34 (1996) 9–16.
[3] A. Cassano, R. Molinari, M. Romano, E. Drioli, Treatment of aqueous effluents of the leather industry by membrane processes: a review, J. Membr. Sci., 181 (2001) 111–126.
[4] C. O'Neill, F. Hawkes, D. Hawkes, N. Lourenco, H. Pinheiro, W. Delee, Colour in textile effluents – sources, measurement, discharge consents and simulation: a review, J. Chem. Technol. Biotechnol., 74 (1999) 1009–1018.
[5] G.C. Kisku, M. Tiwari, S.P. Shukla, D.S. Singh, R.C. Murthy, Characterization and adsorptive capacity of coal fly ash from

aqueous solutions of disperse blue and disperse orange dyes, Environ. Earth Sci., 74 (2015) 1125–1135.
[6] A.A.P. Khan, A. Khan, A.M. Asiri, N. Azuma, M.A. Rub, Micro concentrations of Ru(III) used as homogenous catalyst in the oxidation of levothyroxine by N-bromosuccinimide and the mechanistic pathway, J. Taiwan Inst. Chem. Eng., 45 (2014) 127–133.
[7] C. Chen, E. Nurhayati, Y. Juang, C. Huang, Electrochemical decolorization of dye wastewater by surface-activated boron-doped nanocrystalline diamond electrode, J. Environ. Sci., 45 (2016) 100–107.
[8] A. Walcarius, L. Mercier, Mesoporous organosilica adsorbents:nanoengineered materials for removal of organic and inorganic pollutants, J. Mater. Chem., 20 (2010) 4478–4511.
[9] B.V. Bruggen, C.Vandecasteele, Removal of pollutants from surface water and groundwater by nanofiltration: overview of possible applications in the drinking water industry, Environ. Pollut., 122 (2003) 435–445.
[10] L.K. Posey, M.G. Viegas, A.J. Boucher, C. Wang, K.R. Stambaugh, M.M. Smith, B.G. Carpenter, B.L. Bridges, S.E. Baker, D.A. Perry, Surface-enhanced vibrational and TPD study of nitroaniline isomers, J. Phys. Chem. C, 111 (2007) 12352–12360.
[11] M.R. Sohrabi, M. Ghavami, Photocatalytic degradation of Direct Red 23 dye using UV/$TiO_2$: effect of operational parameters, J. Hazard. Mater., 153 (2008) 1235–1239.
[12] M. Abbasi, N.R. Asl, Sonochemical degradation of Basic Blue 41 dye assisted by nano$TiO_2$ and $H_2O_2$, J. Hazard. Mater., 153 (2008) 942–947.
[13] H. Valdés, H.P. Godoy, C.A. Zaror, Heterogeneous catalytic ozonation of cationic dyes using volcanic sand, Water Sci. Technol., 61 (2010) 2973–2979.
[14] M.X. Zhu, L. Lee, H.H. Wang, Z. Wang, Removal of an anionic dye by adsorption/precipitation processes using alkaline white mud, J. Hazard. Mater., 149 (2007) 735–741.
[15] F. Aktaş, Bioremediation techniques and strategies on removal of polluted environment, J. Eng. Res. Appl. Sci., 2 (2013) 107–115.
[16] A.K. Jain, V.K. Gupta, A. Bhatnagar, Suhas, Utilization of industrial waste products as adsorbents for the removal of dyes, J. Hazard. Mater., 101 (2003) 31–42.
[17] Y.S. Ho, G. McKay, Sorption of dyes and copper ions onto biosorbents, Process Biochem., 38 (2003) 1047–1061.
[18] A.N. Fernandes, C.A.P. Almeida, C.T.B. Menezes, N.A. Debacher, M.M.D. Sierra, Removal of methylene blue from aqueous solution by peat, J. Hazard. Mater., 144 (2007) 412–419.
[19] E.N. El Qada, S.J. Allen, G.M. Walker, Adsorption of basic dyes from aqueous solution onto activated carbons, Chem. Eng. J., 135 (2008) 174–184.
[20] G.G. Stavropoulos, A.A. Zabaniotou, Production and characterization of activated carbons from olive-seed waste residue, Microporous Mesoporous Mater., 82 (2005) 79–85.
[21] B. Bestani, N. Benderdouche, B. Benstaali, M. Belhakem, A. Addou, Methylene blue and iodine adsorption onto an activated desert plant, Bioresour. Technol., 99 (2008) 8441–8444.
[22] M.J. Iqbal, M.N. Ashiq, Adsorption of dyes from aqueous solutions on activated charcoal, J. Hazard. Mater., 139 (2007) 57–66.
[23] A. Kumar, S. Kumar, S. Kumar, D.V. Gupta, Adsorption of phenol and 4 nitrophenol on granular activated carbon in basal salt medium: equilibrium and kinetics, J. Hazard. Mater., 147 (2007) 155–166.
[24] K.Y. Foo, B.H. Hameed, An overview of dye removal via activated carbon adsorption process, Desal. Wat. Treat., 19 (2010) 225–274.
[25] R. Elmoubarki, F.Z. Mahjoubi, H. Tounsadi, J. Moustadraf, M. Abdennouri, A. Zouhri, A. El Albani, N. Barka, Adsorption of textile dyes on raw and decanted Moroccan clays: kinetics, equilibrium and thermodynamics, Water Resour. Ind., 9 (2015) 16–29.
[26] T. Otowa, Y. Nojima, T. Miyazaki, Development of KOH activated high carbon and its application to water purification, Carbon, 35 (1997) 1315–1319.
[27] D. Prahas, Y. Kartika, N. Indraswati, S. Ismadji, Activated carbon from jackfruit peel waste by $H_3PO_4$ chemical activation: pore structure and surface chemistry characterization, Chem. Eng. J., 140 (2008) 32–42.
[28] H. Zaitan, D. Bianchi, O. Achak, T. Chafik, A comparative study of the adsorption and desorption of *o*-xylene onto bentonite clay and alumina, J. Hazard. Mater., 153 (2008) 852–859.
[29] G. Sheng, H. Dong, Y. Li, Characterization of diatomite and its application for the retention of radiocobalt: role of environmental parameters, J. Environ. Radioact., 113 (2012) 108–115.
[30] J.B. Zhang, Y.X. Yang, Z.L. Wang, Z. Huang, Y.R. Chen, Adsorption properties of Zhejiang diatomite modified by supramolecule, J. Dispers. Sci. Technol., 30 (2009) 83–91.
[31] J. Huang, Y. Liu, Q. Jin, X. Wang, J. Yang, Adsorption studies of a water soluble dye, reactive red MF-3B, using sonication-surfactant-modified attapulgite clay, J. Hazard. Mater., 143 (2007) 541–548.
[32] M.M. Abd EL-Latif, A.M. Ibrahim, Adsorption, kinetic and equilibrium studies on removal of basic dye from aqueous solutions using hydrolyzed oak sawdust, Desal. Wat. Treat., 6 (2009) 252–268.
[33] S. Lagergren, About the theory of so-called adsorption of soluble substances, K. Sven vetensk.akad. Handl., 24 (1898) 1–39.
[34] Y.S. Ho, G. McKay, D.A.J. Wase, C.F. Forster, Study of the sorption of divalent metal ions on to peat, Adsorpt. Sci. Technol., 18 (2000) 639–650.
[35] K.W. Foo, B.H. Hameed, Preparation, characterization and evaluation of adsorptive properties of orange peel based activated carbon via microwave induced $K_2CO_3$ activation, Bioresour. Technol., 104 (2012) 679–686.
[36] S. Nethaji, A. Sivasamy, Adsorptive removal of an acid dye by lignocellulosic waste biomass activated carbon: equilibrium and kinetic studies, Chemosphere, 82 (2011) 1367–1372.
[37] J. Fan, J. Zhang, C. Zhang, L. Ren, Q. Shi, Adsorption of 2,4,6-trichlorophenol from aqueous solution onto activated carbon derived from loosestrife, Desalination, 267 (2011) 139–146.
[38] S.J. Allen, G. Mckay, K.Y.H. Khader, Intraparticle diffusion of a basic dye during adsorption onto sphagnum peat, Environ. Pollut., 56 (1989) 39–50.
[39] K.C. Bedin, A.C. Martins, A.L. Cazetta, O. Pezoti, V.C. Almeida, KOH-activated carbon prepared from sucrose spherical carbon: adsorption equilibrium, kinetic and thermodynamic studies for Methylene Blue removal, Chem. Eng. J., 286 (2016) 476–484.
[40] V.K. Gupta, R. Jain, M.N. Siddiqui, T.A. Saleh, S. Agarwal, S. Malati, D. Pathak, Equilibrium and thermodynamic studies on the adsorption of the dye rhodamine-B onto mustard cake and activated carbon, J. Chem. Eng. Data, 55 (2010) 5225–5229.
[41] D. Ozdes, C. Duran, Equilibrium, kinetics, and thermodynamic evaluation of mercury (II) removal from aqueous solutions by moss (*Homalothecium sericeum*) biomass, Environ Prog. Sustain. Energy, 34 (2015) 1620–1628.
[42] P. Turan, M. Dogan, M. Alkan, Uptake of trivalent chromium ions from aquesous solutions using kaoilinite, J. Hazard. Mater., 148 (2007) 56–63.
[43] Z. Sun, C. Li, D. Wu, Removal of methylene blue from aqueous solution by adsorption onto zeolite synthesized from coal fly ash and its thermal regeneration, J. Chem. Technol. Biotechnol., 85 (2010) 845–850.
[44] P.K. Malik, Use of activated carbons prepared from sawdust and rice-husk for sorption of acid dyes: a case study of acid yellow 36, Dyes Pigm., 56 (2003) 239–249.
[45] M.S.U. Rehman, M. Munir, M. Ashfaq, N. Rashid, M.F. Nazar, M. Danish, J.-I. Han, Adsorption of brilliant green dye onto red clay, Chem. Eng. J., 228 (2013) 54–62.
[46] H. Sadegh, R. Shahryari-ghoshekandi, S. Agarwal, I. Tyagi, M. Asif, V.K. Gupta, Microwave-assisted removal of malachite green by carboxylate functionalized multi-walled carbon nanotubes: kinetics and equilibrium study, J. Mol. Liq., 206 (2015) 151–158.
[47] I. Langmuir, Adsorption of gases on plain surfaces of glass mica platinum, J. Am. Chem. Soc., 40 (1918) 1361–1403.
[48] H.M.F. Freundlich, Over the adsorption in solution, Z. Phys. Chem., 57 (1906) 385–470.

[49] O. Redlich, D.L. Peterson, A useful adsorption isotherm, J. Phys. Chem., 63 (1959) 1024–1024.
[50] J. Toth, State equations of the solid gas interface layer, Acta Chem. Acad. Hung., 69 (1971) 311–317.
[51] K.R. Hall, L.C. Eagleton, A. Acrivos, T. Vermeulen, Pore-solid-diffusion kinetics in fixed-bed adsorption under constant-pattern conditions, Ind. Eng. Chem. Res., 5 (1966) 212–216.
[52] T.W. Weber, R.K. Chakravorti, Pore and solid diffusion models for fixed-bed adsorbers, AIChE J., 20 (1974) 228–238.
[53] M. Kumar, B.P. Tripathi, V.K. Shahi, Crosslinked chitosan/polyvinyl alcohol blend beads for removal and recovery of Cd(II) from wastewater, J. Hazard. Mater., 172 (2009) 1041–1048.
[54] V.V. Basava Rao, S.R. Mohan Rao, Adsorption studies on treatment of textile dyeing industrial effluent by fly ash, Chem. Eng. J., 116 (2006) 77–84.
[55] Y.C. Sharma, U.S.N. Upadhyay, An economically viable removal of methylene blue by adsorption on activated carbon prepared from rice husk, Can. J. Chem. Eng., 89 (2011) 377–383.
[56] A. Gurses, S. Karaca, C. Dogar, R. Bayrak, M. Acıkyıldız, M. Yalcın, Determination of adsorptive properties of clay/water system: methylene blue sorption, J. Colloid Interface Sci., 269 (2004) 310–314.
[57] D. Ghosh, K.G. Bhattacharyya, Adsorption of methylene blue on kaolinite, Appl. Clay Sci., 20 (2002) 295–300.
[58] C. Woolard, J. Strong, C. Erasmus, Evaluation of the use of modified coal ash as a potential sorbent for organic waste streams, Appl. Geochem., 17 (2002) 1159–1164.
[59] D. Ozdes, C. Duran, H.B. Senturk, H. Avan, B. Bicer, Kinetics, thermodynamics, and equilibrium evaluation of adsorptive removal of methylene blue onto natural illitic clay mineral, Desal. Wat. Treat., 52 (2014) 208–218.
[60] G. Cheng, L. Sun, L. Jiao, L.-X. Peng, Z.-H. Lei, Y.-X. Wang, J. Lin, Adsorption of methylene blue by residue biochar from copyrolysis of dewatered sewage sludge and pine sawdust, Desal. Wat. Treat., 51 (2013) 7081–7085.
[61] S. Banerjee, M.C. Chattopadhyaya, V. Srivastava, Y.C. Sharma, Adsorption studies of methylene blue onto activated saw dust: kinetics, equilibrium, and thermodynamic studies, Environ. Prog. Sustain. Energy, 33 (2014) 790–799.
[62] Y. Bulut, H. Aydın, A kinetics and thermodynamics study of methylene blue adsorption on wheat shells, Desalination, 194 (2006) 259–267.
[63] M.C. Ncibi, B. Mahjoub, M. Seffen, Kinetic and equilibrium studies of methylene blue biosorption by *Posidonia oceanica* (L.) fibres, J. Hazard. Mater., 139 (2007) 280–285.
[64] H. Lata, V.K. Garg, R.K. Gupta, Removal of a basic dye from aqueous solution by adsorption using *Parthenium hysterophorus*: an agricultural waste, Dyes Pigm., 74 (2007) 653–658.
[65] M.A. Al-Ghouti, M.A.M. Khraisheh, S.J. Allen, M.N. Ahmad, The removal of dyes from textile wastewater: a study of the physical characteristics and adsorption mechanisms of diatomaceous earth, J. Environ. Manage., 69 (2003) 229–238.
[66] B.H. Hameed, Spent tea leaves: a new non-conventional and low-cost adsorbent for removal of basic dye from aqueous solutions, J. Hazard. Mater., 161 (2009) 753–759.
[67] M. Auta, B.H. Hameed, Coalesced chitosan activated carbon composite for batch and fixed-bed adsorption of cationic and anionic dyes, Colloids Surf., B, 105 (2013) 199–206.
[68] M. Peydayesh, A. Rahbar-Kelishami, Adsorption of methylene blue onto *Platanus orientalis* leaf powder: kinetic, equilibrium and thermodynamic studies, J. Ind. Eng. Chem., 21 (2015) 1014–1019.
[69] N. Nasuha, B.H. Hameed, Adsorption of methylene blue from aqueous solution onto NaOH-modified rejected tea, Chem. Eng. J., 166 (2011) 783–786.
[70] S.K. Theydan, M.J. Ahmed, Adsorption of methylene blue onto biomass-based activated carbon by $FeCl_3$ activation: equilibrium, kinetics, and thermodynamic studies, J. Anal. Appl. Pyrolysis, 97 (2012) 116–122.